A new source discriminant based on frequency dispersion for hydroacoustic phases recorded by *T*-phase stations

Jacques Talandier[1] and Emile A. Okal[2]

[1]*CEA-DAM-DIF Commissariat á l'Energie Atomique, F-91297 Arpajon CEDEX, France*
[2]*Department of Earth and Planetary Sciences, Northwestern University, Evanston, IL 60208, USA. E-mail: emile@earth.northwestern.edu*

SUMMARY

In the context of the verification of the Comprehensive Nuclear-Test Ban Treaty in the marine environment, we present a new discriminant based on the empirical observation that hydroacoustic phases recorded at *T*-phase stations from explosive sources in the water column feature a systematic inverse dispersion, with lower frequencies traveling slower, which is absent from signals emanating from earthquake sources. This difference is present even in the case of the so-called 'hotspot earthquakes' occurring inside volcanic edifices featuring steep slopes leading to efficient seismic–acoustic conversions, which can lead to misidentification of such events as explosions when using more classical duration-amplitude discriminants. We propose an algorithm for the compensation of the effect of dispersion over the hydroacoustic path based on a correction to the spectral phase of the ground velocity recorded by the *T*-phase station, computed individually from the dispersion observed on each record. We show that the application of a standard amplitude-duration algorithm to the resulting compensated time-series satisfactorily identifies records from hotspot earthquakes as generated by dislocation sources, and present a full algorithm, lending itself to automation, for the discrimination of explosive and earthquake sources of hydroacoustic signals at *T*-phase stations. The only sources not readily identifiable consist of a handful of complex explosions which occurred in the 1970s, believed to involve the testing of advanced weaponry, and which should be independently identifiable through routine vetting by analysts. While we presently cannot provide a theoretical justification to the observation that only explosive sources generate dispersed *T* phases, we hint that this probably reflects a simpler, and more coherent distribution of acoustic energy among the various modes constituting the wave train, than in the case of dislocation sources embedded in the solid Earth.

Key words: Hydrogeophysics; Pacific Ocean.

1 INTRODUCTION

For the purpose of verification of the Comprehensive Nuclear-Test Ban Treaty (CTBT) in the marine environment, the International Monitoring System (IMS) uses a combination of hydrophones deployed in the SOFAR channel, and of so-called *T*-phase seismic stations. The latter consist of short-period seismometers deployed either on small volcanic islands (e.g. HA09, Tristan da Cunha) or on continental structures in the immediate vicinity of the shoreline (e.g. HA02, Haida Gwaii, Canada), and featuring enhanced response in the frequency band 2–50 Hz. Under such conditions, hydroacoustic energy generated by a natural or artificial source, and traveling inside the SOFAR channel, can be immediately detected before the high-frequency seismic waves into which it converts at a receiving shore suffer anelastic attenuation during propagation in the solid Earth; this effect reduces the domain of effective investigation of *T*-phase station records to the frequency band 2–20 Hz.

In simple terms, the main challenge facing analysts of the IMS consists of defining algorithms allowing the hopefully automated identification of the source (natural or man-made) of signals detected by the network. Despite the occasional incidence of volcanism or acoustic emissions from icebergs, this identification overwhelmingly involves a discrimination between earthquakes and underwater explosions.

In a previous contribution (Talandier & Okal 2001; hereafter Paper I), we examined a data set of 150 *T*-phase signals recorded at seismic stations of the Polynesian Seismic Network (Réseau Sismique Polynésien; hereafter RSP), and devised an empirical source discriminant (*D*, hereafter D_0), allowing the identification of signals generated by underwater explosions and distant earthquakes. Specifically, we then proposed to measure the maximum e_{Max} of the envelope of the ground velocity recorded in the *T* phase at the receiving station (in μm s^{-1}) and the duration $\tau_{1/3}$ during which the envelope is sustained at or above 1/3 of e_{Max} (in
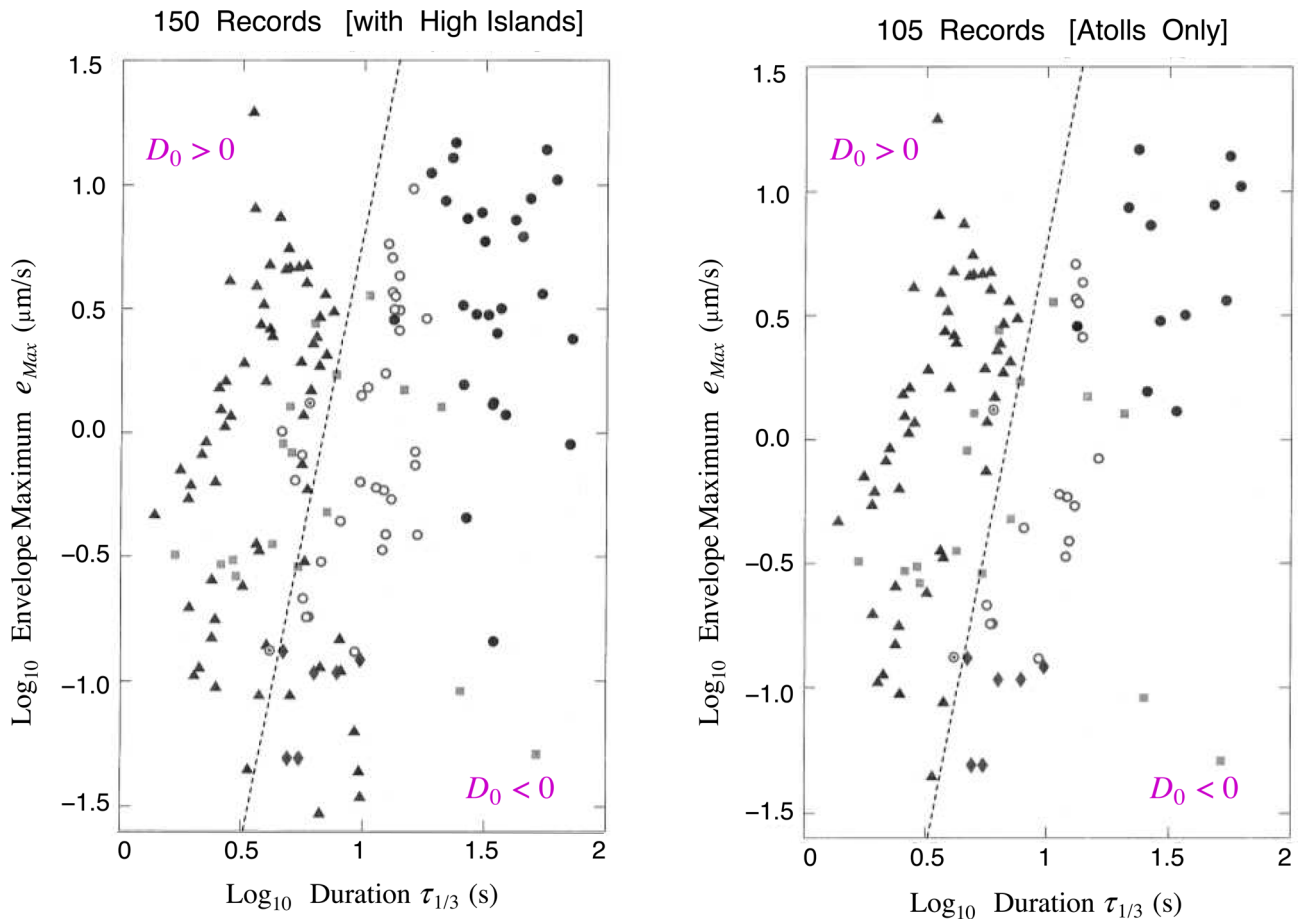
Figure 1. Data set used in Paper I to define the original discriminant D_0. Left: full data set including receivers on high islands. Right: sub-dataset using only atoll stations. On both frames, the dashed line corresponds to $D_0 = 0$, solid triangles represent man-made explosive sources, solid circles subduction zone earthquakes, open circles so-called 'midplate earthquakes', including hotspot events, squares volcanic sources and diamonds presumed firing of missiles. The bull's eye symbols show hotspot earthquakes misidentified by D_0. Adapted from figs 7 and 6 of Paper I.

seconds). Then, our results, summarized on Fig. 1, showed that the quantity

$$D_0 = \log_{10} e_{\text{Max}} - 4.9 \log_{10} \tau_{1/3} + 4.1 \qquad (1)$$

can act as a discriminant effectively separating explosions ($D_0 > 0$) from earthquakes ($D_0 < 0$).

When interpreting the amplitudes of T wave trains at various stations, it is imperative to keep in mind that the final amplitude recorded at any given site is the result of a complex series of processes at the source itself, at the seismic–acoustic conversion point for sources outside the water column, along the path of acoustic propagation, at the acoustic–seismic conversion point, and finally at the receiver itself, when the latter is significantly distant from the converting slope (e.g. de Groot-Hedlin & Orcutt 1999; Bohnenstiehl *et al.* 2012). Thus, and as underscored by Okal *et al.* (2003), the interpretation of absolute amplitudes, or of relative amplitudes recorded at sites with strongly differing environments, can only be tentative. In particular, we pointed out in Paper I that the performance of the discriminant D_0 was considerably improved by restricting its application to receivers located on atolls, where steep water–solid interfaces lead to a more efficient and faster acoustic-to-seismic conversion than at the shallow-dipping slopes characteristic of the so-called 'high islands' (Okal 2001). At the latter, which feature a recent, emerged volcanic structure, acoustic–seismic conversion involves the receiver counterpart of the classical and complex

source-side downslope conversion process (Johnson *et al.* 1963; Talandier & Okal 1998); for this reason, this study will use exclusively receivers located on atolls.

We proposed in Paper I a very general explanation of the discriminant D_0, based on the concept of scaling laws relating both the amplitude and the duration of an acoustic wave in the water to the size of the source. For physical sources as different as an earthquake dislocation and an explosion in the water, we were able to justify a difference in the relative growth of amplitude and duration, and to predict a difference in the relative scaling of e_{Max} to $\tau_{1/3}$.

However, Paper I raised a number of questions, and in particular the case of the so-called 'hotspot earthquakes', occurring inside volcanic edifices such as the island of Hawaii or the small active island of Mehetia in the Society chain. Records from several such events were misidentified by the discriminant D_0, on account of the possibility of a highly efficient source-side seismic-to-acoustic conversion (both in terms of amplitude and short duration) if the seismic source is located in the immediate vicinity of a steep island slope at depths typical of the SOFAR channel.

The purpose of this study is to report on a new discriminant allowing an efficient separation of explosive sources from earthquakes, including 'hotspot earthquakes', based on the empirical observation that the former exhibit a systematic inverse dispersion of their wave trains, while the latter do not. This investigation is carried over an extended data set including in particular a more diverse distribution

of earthquake sources. However, we strictly restrict ourselves to receivers located on atolls, and in the end, the dimension of the new data set, consisting of 146 records, is essentially unchanged from that used in Paper I. In addition, and as described in detail in the following section, the systematic operational use of the amplitude-duration criterion (1) has led to a slight alteration of its algorithm.

2 THE AMPLITUDE-DURATION DISCRIMINANT: AN UPDATE

The continuous operational use of the discriminant D_0 at the Laboratoire de Géophysique in Papeete has led to a slight revision of its algorithm, in order to increase its performance for small and especially short events. Specifically, under the D_0 algorithm defined in Paper I, the quantification of the envelope was performed by filtering the ground velocity time series at $f \geq 2$ Hz, redressing the signal and smoothing it through a 1-s sliding window. It was found, however, that this procedure artificially lengthened the parameter $\tau_{1/3}$ of the smallest signals, whose true duration could be comparable to the length of the sliding window. As a result, we now use a shorter sliding window, lasting only 0.4 s. Under this new algorithm, the coefficients used in the discriminant D must be slightly retouched, and we now use

$$D_1 = \log_{10} e_{\text{Max}} - 5.0 \log_{10} \tau_{1/3} + 4.53 \tag{2}$$

where the new values of e_{Max} and $\tau_{1/3}$ are derived using the shorter sliding window.

The data set analysed in this study comprises a subset of records used in Paper I, namely those obtained at stations of the RSP located on atolls (e.g. Rangiroa). These stations are deployed in the immediate vicinity (mostly 50 m, never more than 200 m) of the steep coral structure in direct contact with the oceanic column transmitting the acoustic wave. Thus, they feature the general characteristics of the so-called 'T-phase stations' mandated under the CTBT (e.g. Okal 2001), of which they are in fact early prototypes.

Of the 150 records used in Paper I (164 including high-energy events not considered in this study), 48 were obtained at other RSP stations, located on so-called 'high islands', that is, on active volcanic structures (Mehetia) or on young basaltic structures whose erosion has not yet reached the underwater stage (e.g. Tahiti, Rikitea, Tubuai), and were eliminated from this study. We further eliminated the six records ('M' in the classification of Paper I) interpreted as presumed submarine missile firings at sea and 15 records emanating from volcanic sources. The latter are generally easily discriminated based on a combination of their location at known centres of volcanism, and on their occurrence during prolonged swarms of activity.

The legacy data set from Paper I thus consists of 81 records; we complement it here by an additional 65 records, mostly obtained through routine monitoring at the Laboratoire de Géophysique in Papeete, but including as well a few records at IRIS stations recently deployed on Pacific atolls such as Christmas Island or Midway. Earthquake records involve sources with reported magnitudes (m_b or M_s) ranging from 3.1 to 6.4; records from explosions with published source parameters involve depths from 50 to 220 m, and yields from 25 to 2000 kg.

In the following sections, we discuss separately the performance of the new discriminant D_1 on various families of events. For each family, we give the minimum and maximum values of D_1, as well as its mean and standard deviation.

2.1 Underwater chemical explosions (E); 71 records; symbol: upward pointing triangle

$$\bar{D}_1 = 2.58 \pm 1.01 \qquad 0.78 \leq D_1 \leq 5.69$$

We combine a subset of 49 events from Paper I with an additional 22 records, primarily from a seismic refraction campaign off Washington State (Taber & Lewis 1986), but also including recent explosions Southwest of Oahu in 2000 (Reymond *et al.* 2003) and off Vancouver Island in 2007. All (E) type sources are identified as underwater explosions, either announced or having been previously described as such in the literature. All values of the discriminant D_1 for these events remain strictly positive (Fig. 2a).

2.2 Complex explosions (C); 17 records; symbol: left pointing triangle

$$\bar{D}_1 = 2.50 \pm 1.80 \qquad 0.11 \leq D_1 \leq 5.20$$

We report here on a series of signals, occurring as gusts and recorded at the RSP in 1971 and 1978, which are interpreted as complex explosions. We study 17 such records, obtained during four sequences, each lasting from a few minutes to a few hours. The signals share with traditional chemical explosions (E) a spectrum rich in high frequencies, and a strong dispersion of their spectrum with frequency. On the other hand, their duration is significantly longer than for signals of the (E) class above, and the buildup of their amplitude can be emergent, to the extent that the discriminant D_1 can become close to zero for the most complex ones (Fig. 2b). This could lead to the misidentification of their sources as earthquake dislocations. It is believed that these signals originated in underwater tests of advanced weaponry in the Northern Pacific.

### 2.3 Subduction zone earthquakes (S); 19 records; symbol: solid square

$$\bar{D}_1 = -2.00 \pm 0.95 \qquad -3.37 \leq D_1 \leq -0.34$$

T phases are recorded routinely from the large population of subduction zone earthquakes taking place daily along the rim of the Pacific Ocean. The data set transferred from Paper I, which included only seven such records at atoll stations, is complemented by 12 new records from subduction earthquakes. Fig. 2(c) confirms the results of Paper I, all records featuring a strongly negative discriminant D_1.

2.4 Transform Fault events (F); 7 (+1) records; symbol: down-pointing triangle

$$\bar{D}_1 = -2.20 \pm 0.83 \qquad -3.64 \leq D_1 \leq -1.02$$

In Paper I, our data set of plate boundary earthquakes comprised four records at atoll stations from strike-slip events, two each on the Mendocino and Eltanin Transform Fault systems. In this study, we consider three more such events from the Eltanin area, and examine the resulting data set separately from its subduction counterpart. We are motivated by Dziak's (2001) observation that strike-slip sources are particularly efficient T-wave generators in the Northeast Pacific Ocean. On this admittedly small data set, we fail to identify a behaviour of D_1 differing significantly from the subduction values. Our results do not allow a clear separation of the two populations, given their respective scatter (Fig. 2d). The two Mendocino records show no particular trend despite the different orientation of their incident acoustic waves in Polynesia.
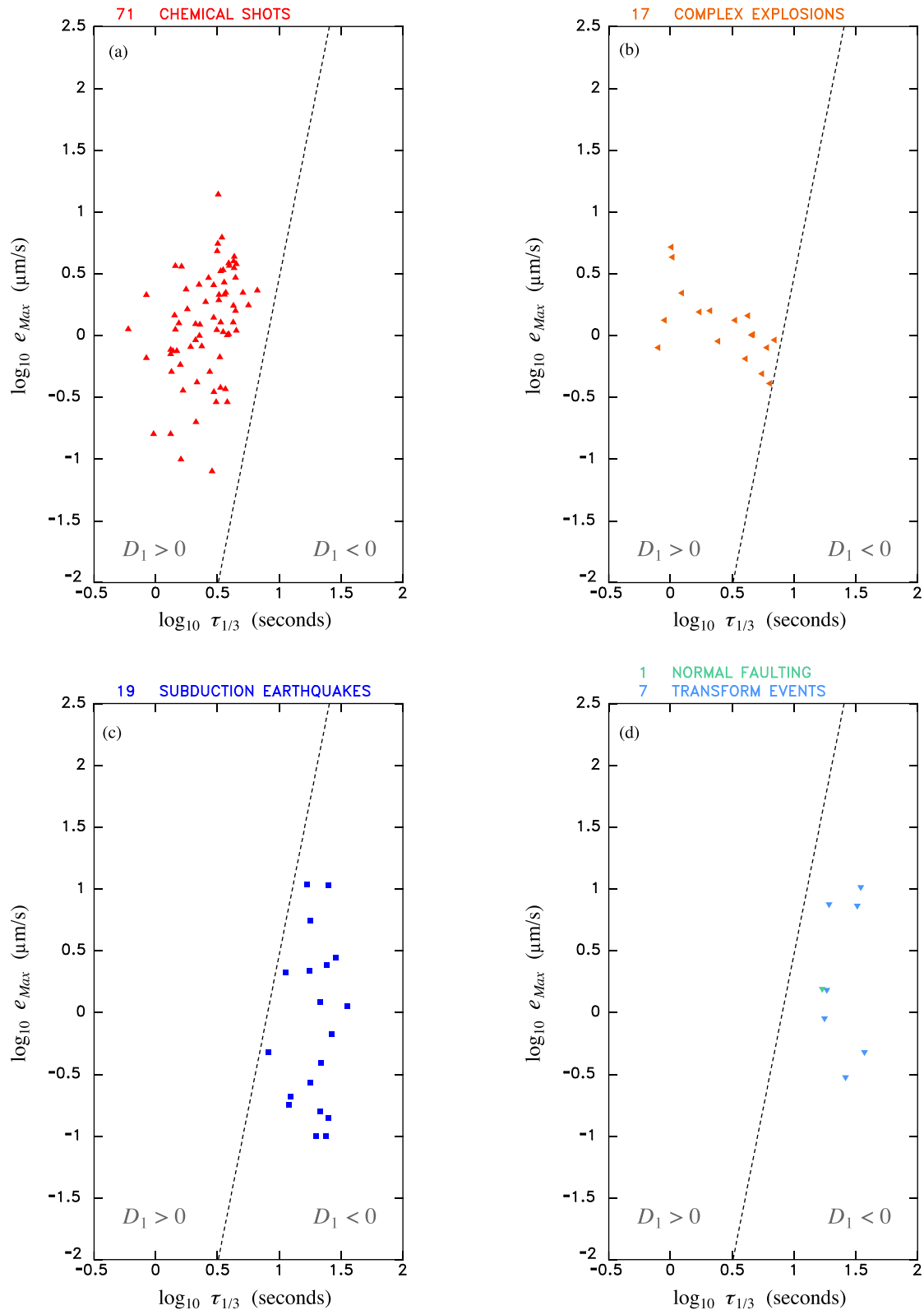
Figure 2. (a) Performance of the discriminant D_1 for the 71 chemical explosion records included in the present data set. D_1 vanishes along the dashed line. Note that all values of D_1 remain positive, above the dashed line representing $D_1 = 0$. (b) Same as (a) for the 17 complex explosion records included in the present data set. Note that all values of D_1 remain positive. (c) Same as (a) for the 19 subduction earthquake records included in the present data set. Note that all values of D_1 remain negative. (d) Same as (a) for the seven transform fault earthquake records (and the lone normal faulting event record) included in the present data set. Note that all values of D_1 remain negative.

We examined separately the case of a large anomalous normal faulting earthquake occurring on the Eltanin system (Okal & Langenhorst 2000; Beutel & Okal 2003), recorded at four different Pacific sites. We find that it cannot be readily distinguished from the rest of the (F) data set ($\bar{D}_1 = -1.42$).

2.5 Hotspot earthquakes (H); 31 records; symbol: open circle

$\bar{D}_1 = 0.27 \pm 1.02$ $\qquad -2.18 \leq D_1 \leq 2.62$

In Paper I, we identified the particular challenge posed, in terms of discrimination, by earthquakes occurring within edifices featuring steep submarines slopes, where seismic-to-acoustic conversion can be particularly efficient (Talandier & Okal 1998). As our examples were drawn from events in the volcanic edifices of the Society and Hawaiian chains, we used the term 'hotspot earthquakes' to describe them. Our original data set included three cases of earthquakes featuring either positive values of D_0 (0.41, 0.22), which would result in a misidentification of these events as explosions, or an essentially null D_0 (−0.12). On the other hand, several records of other Hawaiian earthquakes had D_0 values comparable to those for subduction zone events.

We add to the 18 records obtained on atolls and used in Paper I, a supplementary data set of 13 new records from Hawaiian earthquakes. The problem of the identification of hotspot earthquakes is dramatically expressed by the excursion of D_1 across the null value, from a minimum of −2.18 to a maximum of 2.62, its mean value, $\bar{D}_1 = 0.27$ being positive, and thus in the field of presumed explosions. Indeed, Fig. 3 shows that the data set features more positive values of D_1 (19) than negative ones (12).

3 FREQUENCY DISPERSION IN THE SPECTRA OF EXPLOSIVE SOURCES

More than a decade of routine monitoring of T phases recorded on Polynesian atolls has revealed a remarkable property, which bears significant promise as a possible discriminant of man-made explosions versus earthquake sources, notably regarding the case of hotspot earthquakes, for which the discriminant D_1 may fail, as described in the previous section.

Namely, hydroacoustic signals generated by explosive sources in the water column systematically feature an inverse dispersion (with lower frequencies traveling slower than higher ones), which is absent from signals emanating from earthquakes. Fig. 4 demonstrates this property by comparing records at Tiputa, Rangiroa (TPT) from the Hawaiian earthquake of 1996 July 23 ((a); $m_b = 4.6$; $M_D = 4.8$), and from an explosion (with a yield of 544 kg) off the coast of Washington (b), part of a campaign of seismic refraction (Taber & Lewis 1986). On each frame, the blue line represents the envelope of the signal band-pass filtered at high frequencies ($8 \leq f \leq 10$ Hz) and the red one at low frequencies ($4 \leq f \leq 5$ Hz). The explosion signal clearly features a delay of approximately 1.5 s of the latter with respect to the former, which is absent from the earthquake signal. This property is also apparent in the time-domain series (plotted in black in the background), and is confirmed by the spectrogram analysis shown on Fig. 5.

Regrettably, we must emphasize that at present, we can offer no rational justification for the origin of this difference in observed dispersion. One possible explanation may be sought in the nature of the hydroacoustic waveform itself, which has long been known to consists of the superposition of many modes sampling the water column
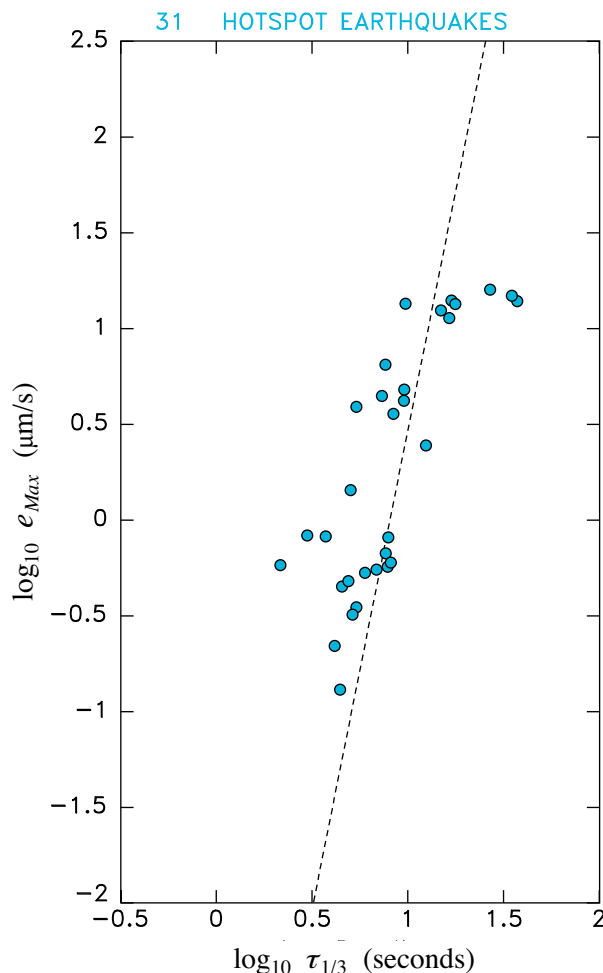
Figure 3. Performance of the discriminant D_1 for the 31 hotspot earthquake records included in the present data set. Note that the values of D_1 straddle the null line, indicating failure of the discriminant D_1 to properly identify such events.

in different ways, and featuring different forms of dispersion, both direct and inverse. We refer, for example, to the pioneering work of Pekeris (1948; in particular his three-layer oceanic model, as also summarized by Ewing *et al.* 1957), and to more modern investigations, such as Piserchia's (1998) or Park *et al.*'s (2001). A different distribution of energy among various modes, from explosive sources in the water as opposed to dislocations in the solid Earth, may result in the presence of coherent dispersion in the former case, and in its absence in the latter. We emphasize however, that any explanation of the generation of T phases by earthquake sources, located outside the oceanic column, must transcend the model of geometrical optics in a simple, laterally homogeneous, stratified medium, since just as acoustic energy cannot escape a waveguide beyond critical incidence, neither can it penetrate it. This longstanding 'T-phase problem' requires generation of acoustic energy either by multiple downslope reflections (Tolstoy & Ewing 1950; Johnson *et al.* 1963; Talandier & Okal 1998), or by scattering from structural heterogeneities at the water–solid interface (de Groot-Hedlin & Orcutt 1999, 2001; Park *et al.* 2001; Yang & Forsyth 2003; Williams *et al.* 2006). Similarly, recording of SOFAR-propagated energy by ocean-bottom sensors deployed deeper than the bottom of the waveguide requires scattering by receiver-side heterogeneities (Stephen *et al.* 2013).
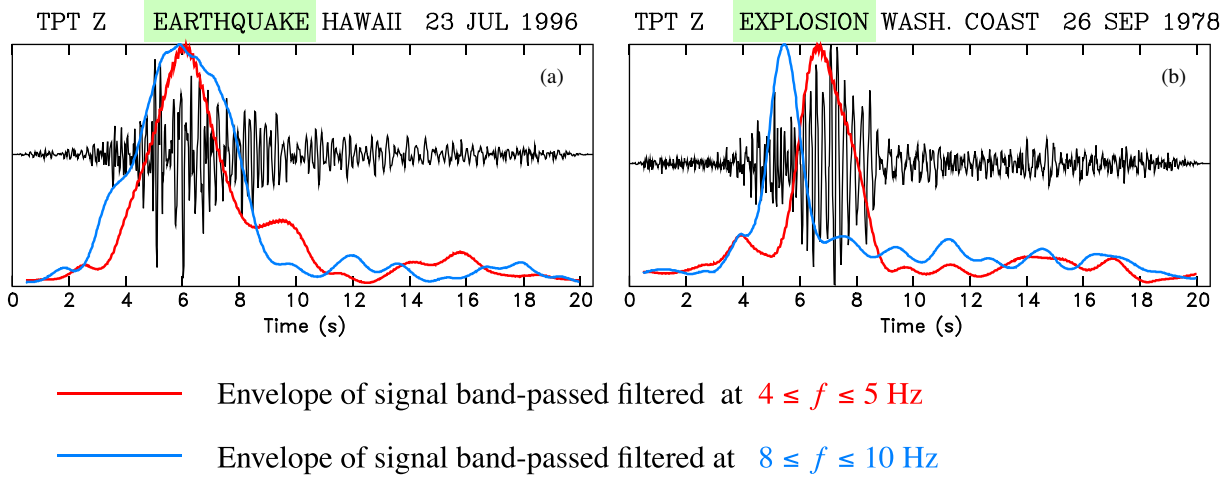
Figure 4. Comparison of hydroacoustic wave trains from (a) an earthquake source and (b) a man-made explosion. On both frames, the red trace represents the envelope of the signal after bandpass filtering at high frequency ($8 \leq f \leq 10$ Hz) and the blue one at low frequency ($4 \leq f \leq 5$ Hz). Note the inverse dispersion clearly present in the explosion signal but absent from the earthquake one.

Nevertheless, and given the overwhelming evidence of the systematic dispersion of signals emanating from explosions in the water column, it seems warranted to devise a methodology allowing the automatic processing of this property as a means of implementing a new algorithm which might successfully discriminate between explosions and seismic events, including those 'hotspot earthquakes' not identified by the discriminant D_1. While the present lack of a theoretical justification remains a substantial reservation to any such methodology, it is hoped that future theoretical and analytical work may shed new light on the physical principles which may eventually provide such a justification.

4 COMPENSATION OF FREQUENCY DISPERSION: TOWARDS A NEW DISCRIMINANT

Our approach towards a new discriminant capable of successfully identifying 'hotspot earthquakes' consists of effecting a compensation of the dispersion through the following algorithm. Note that for the dispersion to be detectable and robustly defined, the minimum epicentral distance will be fixed at 1500 km.

(i) We use a variable bandpass filtering technique to define the dispersion, as measured by the arrival time in the recorded time-series of a particular frequency. This measurement obviously expresses the dispersion as a group velocity, $U(\omega)$. In practice, we found that a relationship of the form

$$U(\omega) = U_\infty - \frac{A}{\omega^p} \tag{3}$$

provides an acceptable fit to our empirically derived dispersion curves, with typical values of $U_\infty = 1483.4$ m s^{-1}, $A = 113$ and $p = 1.7$ if ω is expressed in rad s^{-1} and U in m s^{-1}. The latter two are simply obtained by optimization of the resulting fit of $U(\omega)$ through a grid search procedure.

(ii) We then express the dispersion as a phase velocity $C(\omega)$, by using the relationship

$$\frac{1}{C(\omega)} = \frac{1}{C_\infty} - \frac{1}{\omega} \int_\omega^\infty \frac{d\omega'}{U(\omega')} \tag{4}$$

which is easily derived from the definitions $C(\omega) = \frac{\omega}{k}$; $U(\omega) = \frac{d\omega}{dk}$, where k is the wavenumber. Once $U(\omega)$ is known, $C(\omega)$ can be, at

least in principle, computed from (4), with the high-frequency limit $C_\infty = U_\infty = 1483.4$ m s^{-1} corresponding to the average value of the sound velocity along the axis of the SOFAR in the Pacific Basin. However, a computational problem arises, since the bound of this integral is infinite. In this context, we rewrite (4) as a function of wavelength Λ and period T, which both go to zero for the same physical integral bound. Eq. (4) is then replaced by the system

$$C(T) = \frac{\Lambda}{T}; \quad \frac{d\Lambda}{dT} = \frac{C^2}{U} \tag{5}$$

which can be integrated numerically after discretization, from the high-frequency bound $\Lambda = 0$, $T = 0$ and $C = C_\infty$.

(iii) Once the dispersion has been expressed as a variation of phase velocity $C(\omega)$ with frequency, it is possible to compensate its effect along a path of length x from source to receiver by artificially correcting the spectral phase of the signal. Specifically, starting with the original ground velocity time-series $y(t)$, we consider its Fourier spectrum

$$Y(\omega) = \int_{-\infty}^{\infty} y(t) \cdot e^{-i\omega t} \cdot dt \tag{6}$$

and correct the spectral phase in the amount $kx = \frac{\omega x}{C(\omega)}$ to obtain a compensated spectrum

$$Z(\omega) = Y(\omega) \cdot e^{\frac{i\omega x}{C(\omega)}} \tag{7}$$

which can be transformed back into the time domain as

$$z(t) = \frac{1}{2\pi} \int_{-\infty}^{\infty} Y(\omega) \cdot e^{\frac{i\omega x}{C(\omega)}} \cdot e^{i\omega t} \cdot d\omega \tag{8}$$

The time-series $z(t)$ then represents the original signal, corrected for the effect of the frequency dispersion featured in the original signal $y(t)$. Examples of this procedure are given in Fig. 6. Note that because of the geographical variation of the structure of the SOFAR channel throughout the Pacific Basin, it is impossible to use a universal expression of the dispersion law, but rather necessary to tailor it to the particular path under study. In this respect, our algorithm can be viewed as performing a compensation for the best-fitting dispersion of the form (3).

(iv) This new compensated time-series $z(t)$ can lend itself to analysis of its duration and envelope amplitude, along the same lines used to compute the discriminant D_1. We can thus define the

CHEMICAL SHOT, Vancouver Is., 21-AUG-1980
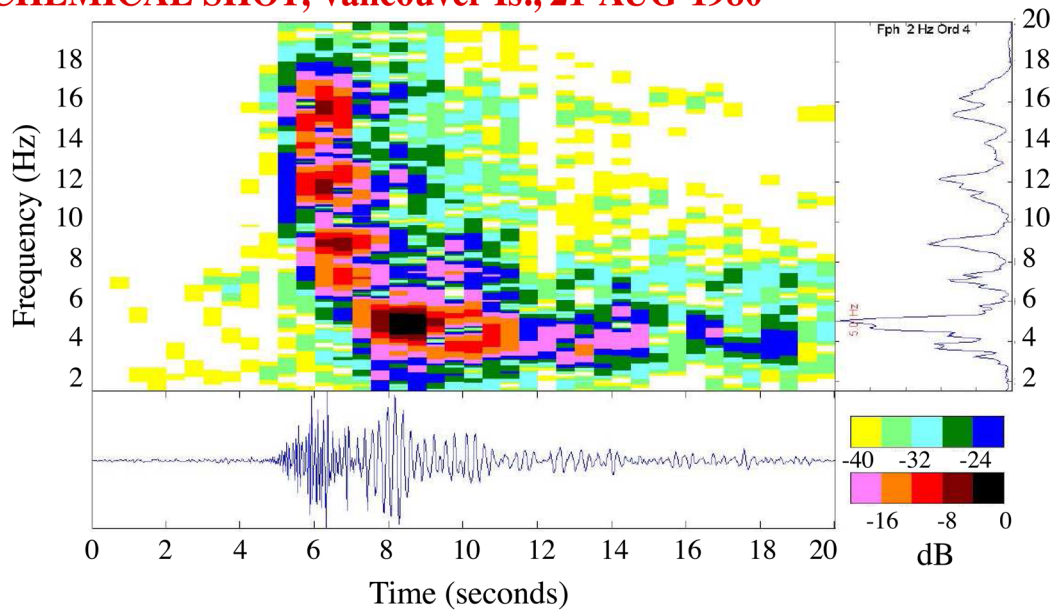
"HOTSPOT" E.Q. Hawaii, 16-MAR-1997
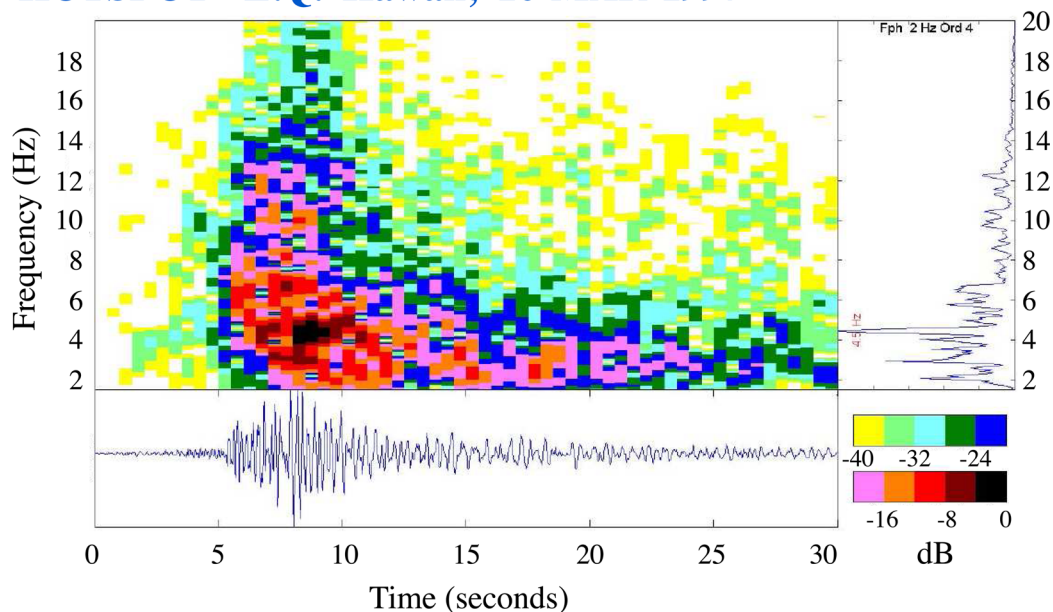
Figure 5. Spectrograms of typical signals recorded from (top) a 2000-kg man-made explosion and (bottom) a so-called 'hotspot earthquake' ($m_b = 4.2$) for which the discriminant D_1 remains positive. Note the clean inverse dispersion for the explosion signal, compared with the more confused repartition of spectral components with time in the case of the earthquake signal.

new parameters $e_{Max}^{Comp.}$ and $\tau_{1/3}^{Comp.}$, where the superscript Comp. underlines the compensated nature of $z(t)$.

5 THE QUEST FOR A NEW DISCRIMINATION ALGORITHM

The goal of discrimination algorithms, notably in the framework of the verification of the CTBT, remains the correct identification of explosive sources. In this respect, we have shown in Section 2 that the discriminant D_1 can be used successfully to rule out an explosive nature for any signal featuring $D_1 < 0$. In our original

data set of 146 records, we find 39 such cases (20 from subduction earthquakes, 7 from ridge earthquakes and 12 from 'hotspot earthquakes'). We also eliminate from further study 24 records obtained at distances less than 1500 km, which are insufficient for an appropriate study of their dispersion characteristics. We are thus left with a new data set of 84 records (51 from chemical shots, 17 from complex explosions and 16 from 'hotspot earthquakes'), for which the compensation procedure described in Section 4 was implemented, and the corresponding parameters $e_{Max}^{Comp.}$ and $\tau_{1/3}^{Comp.}$ evaluated.

Results are presented on Fig. 7. The left frame shows the subset of D_1 values (obviously all negative) for the reduced data set of 84 records. Note that D_1 cannot reliably discriminate signals from
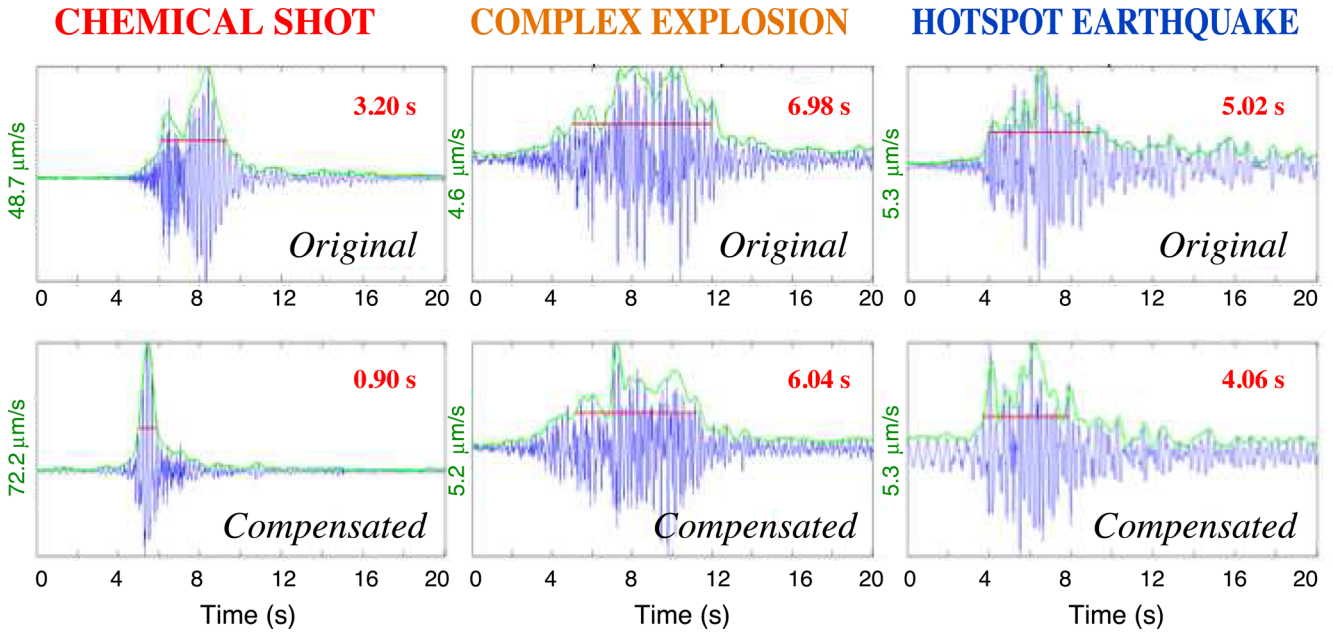
Figure 6. Examples of the procedure of compensation of the frequency dispersion on typical signals from a classical water explosion (left; 1980 August 21, yield 2000 kg), a 'complex explosion' (centre; 1971 August 17) and a 'hotspot earthquake' (right; 1997 March 16, Kilauea, Hawaii, $h = 8$ km and $m_b = 4.2$). The top frames show the original signals $y(t)$ and the bottom ones the compensated signals $z(t)$. In each frame, the green curve represents the envelope used in the calculation of e_{Max} (or $e_{Max}^{Comp.}$) and the red bar defines the duration $\tau_{1/3}$ (or $\tau_{1/3}^{Comp.}$). Note that the procedure of compensation reduces considerably the duration of the explosion signal, but has a substantially lesser effect on the other two.

$$D_1 = \log_{10} e_{Max} - 5.0 \log_{10} \tau_{1/3} + 4.53$$
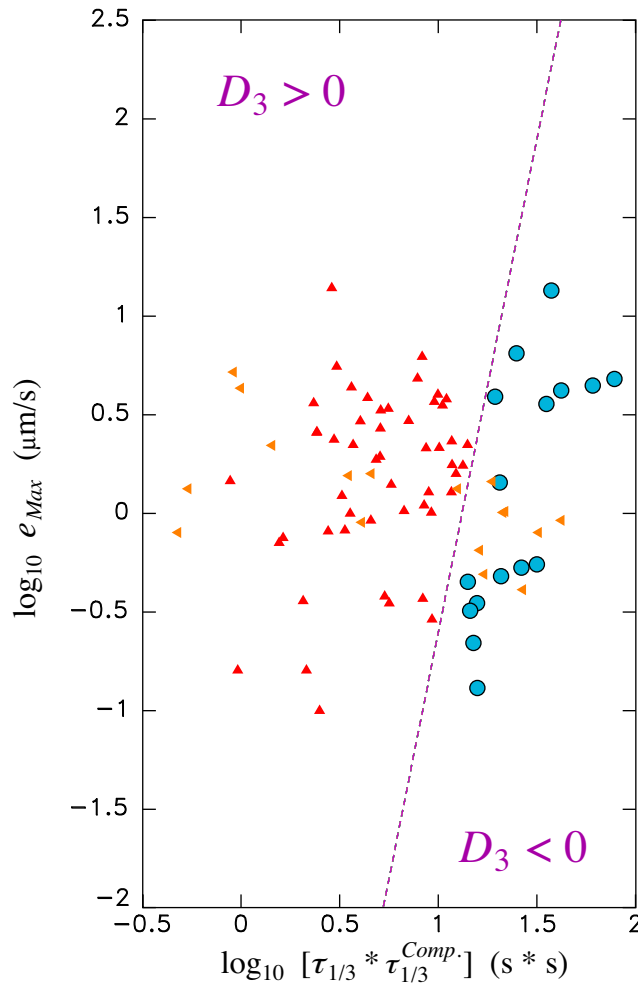
$$D_2 = \log_{10} e_{Max} - 5.0 \log_{10} \tau_{1/3}^{Comp.} + 2.48$$
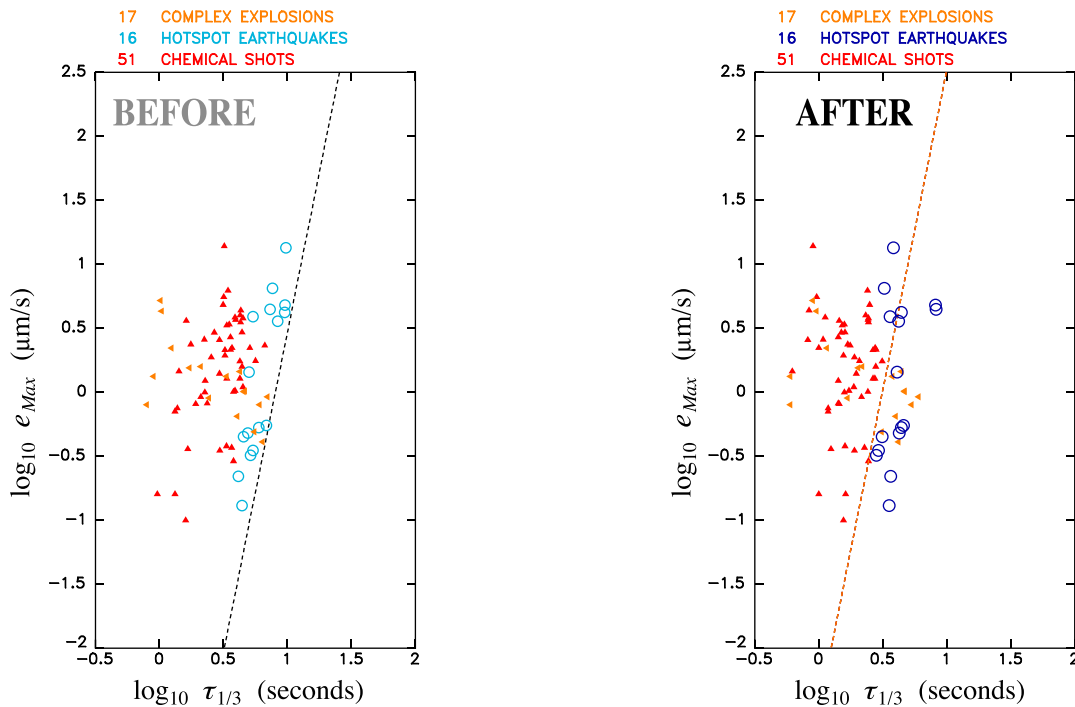
Figure 7. Performance of the discriminants D_1 and D_2 for the sub-dataset of 84 records targeted for compensation of frequency dispersion. Records from chemical shots are shown are upwards-pointing triangles, from complex explosions as left-pointing triangles, and from 'hotspot earthquakes' as open circles. Left: discriminant D_1 (before compensation); note that all values are positive for this sub-dataset, since a negative value rules out a possible explosion. Right: discriminant D_2 (after compensation; defined by (9)). Note that all but three 'hotspot earthquake' signals now feature a negative discriminant, but that many complex explosion signals also move across the null line.

Figure 8. Performance of the discriminant D_3 defined by (10) on the sub-dataset of 84 records targeted for compensation of frequency dispersion. Note that all 'hotspot earthquake' records (open circles) now feature a negative D_3, which separates them reliably from those of chemical shots (upwards-pointing triangles). However, complex explosions (left-pointing triangles) cannot be identified. See the text for details.

'hotspot earthquakes'. In practice, and in most cases, the value $e_{\mathrm{Max}}^{\mathrm{Comp.}}$ differs only slightly (less than a factor 1.5 or 0.2 logarithmic units) from the uncompensated value, while more significant differences occur for the duration $\tau_{1/3}^{\mathrm{Comp.}}$. Thus, on the right frame, we plot the uncompensated value e_{Max} as a function of the compensated duration $\tau_{1/3}^{\mathrm{Comp.}}$, from the time-series $z(t)$. We define a new discriminant D_2 through

$$D_2 = \log_{10} e_{\mathrm{Max}} - 5.0 \log_{10} \tau_{1/3}^{\mathrm{Comp.}} + 2.48. \tag{9}$$

In this formula, the slope (5.0) of the power law has been kept, and the final constant (2.48) adjusted to attempt the optimal separation between the populations of signals from hotspot earthquakes and explosions. While some improvement is clear, three earthquake signals still are not resolved. In addition, we note that many complex explosions signals revert to a negative discriminant D_2, and hence to the 'earthquake domain'.

Finally, we propose to empirically build a discriminant D_3 as

$$D_3 = \log_{10} e_{\mathrm{Max}} - 5.0 \log_{10}[\tau_{1/3} * \tau_{1/3}^{\mathrm{Comp.}}] + 5.60 \tag{10}$$

which geometrically combines the original and compensated durations of the signals. Fig. 8 shows that this algorithm successfully separates hotspot earthquake signals (which now all feature $D_3 < 0$) and explosion ones ($D_3 > 0$). We have verified that the use of $e_{\mathrm{Max}}^{\mathrm{Comp.}}$ instead of e_{Max} in (10) does not change this result.

6 DISCUSSION AND CONCLUSIONS

We observe an empirical difference in dispersion of hydroacoustic far-field signals generated by explosions and earthquakes (including the so-called 'hotspot earthquakes' not properly identified by the original amplitude-duration discriminant D_1). While the former sources are characterized by a well-defined inverse dispersion in the range 3.5–10 Hz, the latter feature a complex, often confuse repartition of frequency components with time, which does not lend itself to a satisfactory description in terms of a single branch of dispersive propagation. This remark, for which we presently offer no theoretical justification, sets the stage for an algorithm of compensation of the relevant dispersion, which can lead, in the case of explosive signals, to a significant shortening of the duration when measured
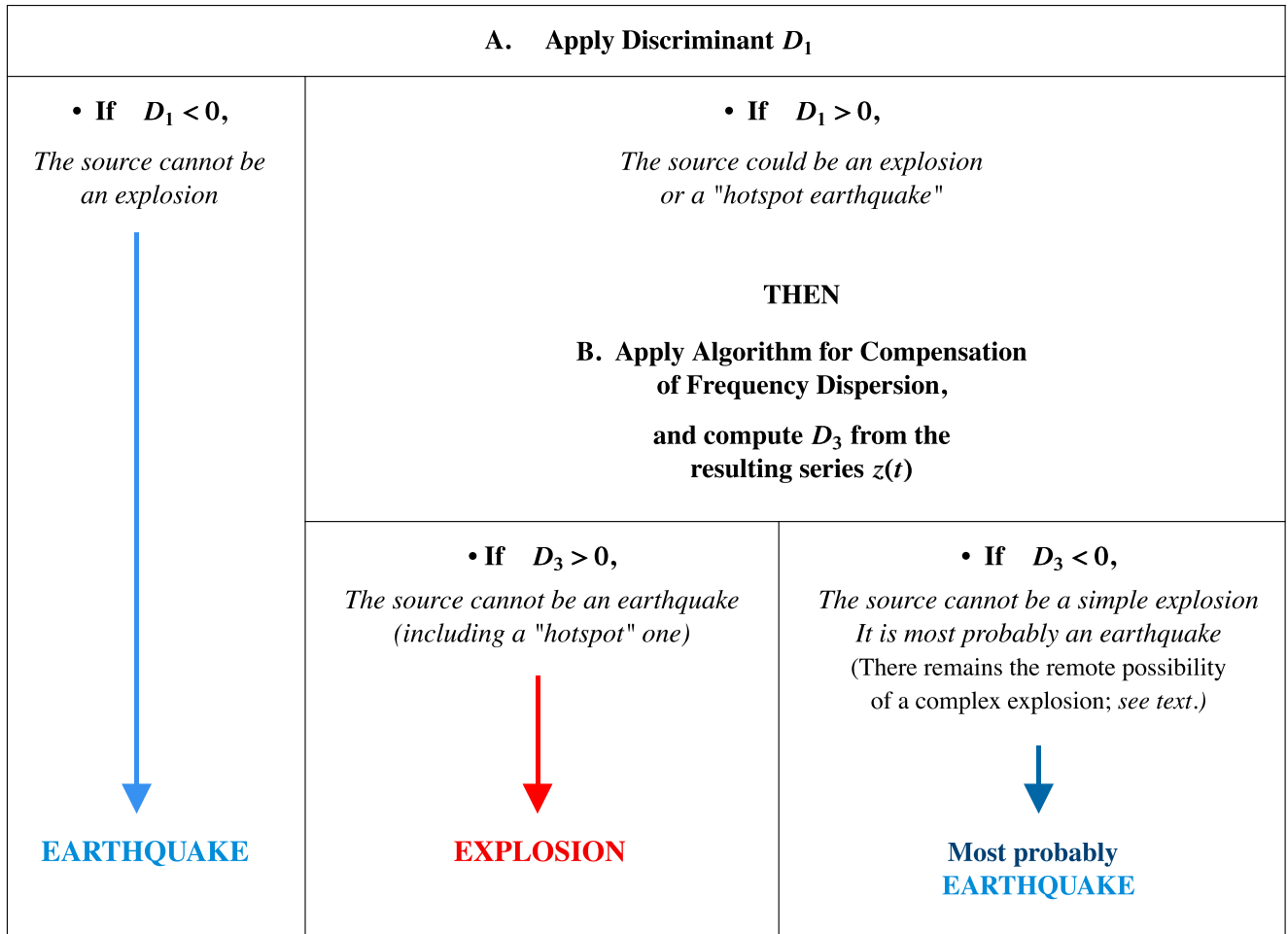
Figure 9. Final proposed algorithm for the discrimination of explosion and earthquake signals at distant ($\Delta > 1500$ km) atoll stations.

on the corrected time-series $z(t)$. As described in Section 5, the outcome of this methodology is the development of the discriminant D_3 given by (10), which satisfactorily resolves the problem of the 'hotspot earthquakes' which could not be identified by D_1.

In this framework, the algorithm described on Fig. 9 can be used as a global identifier of man-made explosions in the oceanic environment: first, use the original duration-amplitude criterion defined in Paper I, slightly retouched in the form of the discriminant D_1. If D_1 is negative, the source cannot be an explosion, and has to be an earthquake. If D_1 is positive, then proceed to perform the dispersion compensation using the algorithm defined in Section 4, and apply the discriminant D_3 to the resulting corrected time-series $z(t)$. If D_3 is positive, then the source has to be an explosion; it cannot be an earthquake, even a so-called 'hotspot' one. If D_3 is negative, the source is most probably an earthquake, but there remains the small probability that it could be a complex explosion. This case is described in the next section.

6.1 The case of the so-called 'Complex Explosions'

Unfortunately, complex explosions, which feature $D_1 > 0$ but can have either positive or negative values of D_3, are not identified by the algorithm on Fig. 9. They constitute the only man-made sources whose signals are not reliably separated from those of earthquakes, and could therefore be mistaken for earthquake signals. However, under an operational perspective, we note that this group consists of 17 records obtained in 1971 and 1978, originating from the deep basins of the Northern Pacific, and occurring in sequences lasting tens of minutes to several hours. No such signals have been recorded at the RSP for the past 37 yr. These characteristics make it very unlikely that such sources could be misidentified as earthquakes in an operational context involving human vetting by an analyst.

6.2 Other sources of hydroacoustic signals not considered in this study

As mentioned in Paper I, a large number of additional hydroacoustic signals are received at the RSP, notably from episodes of volcanism in the Pacific Basin. Because of the large diversity of physical phenomena involved during a volcanic eruption (including *bona fide* earthquakes occurring within the volcanic edifice and magmatophreatic explosions at the contact between lava and sea water), these signals offer a wide variety of characteristics, notably positive as well as negative values of the various discriminants described in this study. The analysis of precise epicentral locations, as well as of their patterns of occurrence (most often in the form of swarms lasting days or weeks), generally allows an analyst of the RSP to identify such signals independently of the algorithms described here.

Finally, drifting icebergs can be the source of hydroacoustic signals (Talandier *et al.* 2002), which may pose an additional challenge in terms of identification, notably when they approach their demise

in the eddy-prone Polar Front around 55°S (e.g. Talandier *et al.* 2006). While they often feature positive values of D_1, and thus could be mistaken for man-made explosions, the dispersion of their signals is generally far from simple, resulting in negative values of the discriminant D_3. This behaviour, essentially similar to that of 'hotspot earthquakes', coupled to their location in extremely remote parts of the Pacific Basin, allows their discrimination from explosive sources.

6.3 Future challenges and directions for further work

As mentioned above, we presently do not have a theoretical understanding of the physical origin of the difference in dispersion patterns between man-made explosions and earthquakes. Further insight could be gained in this respect through the study of records from underground (nuclear) tests, which combine an explosive nature with a source located in the solid Earth. In addition, the use of hydrophone records could, at least in principle, eliminate any possible influence of receiver-side acoustic–seismic conversions, even though the deployment of RSP atoll stations within 50 m of the shore line (i.e. within a fraction of the relevant wavelengths) minimizes this effect. Furthermore, as documented, for example, by Walker *et al.* (1992), little spectral power is present in earthquake signals recorded on hydrophones beyond 18 Hz, which constitutes the limit of our investigations using RSP stations. In the case of explosive sources, the dispersion described in the present work is expressed in the form of a group delay of the lowest frequency components of the spectrum (4–5 Hz on Fig. 6); dispersion is already essentially absent between 8 and 18 Hz (Fig. 5; top), which suggests that there would be little advantage to exploring even higher frequencies.

In parallel, it would be hoped that the extension of the proposed discrimination algorithm to receivers located in different geographic provinces could test its robustness, and in particular that of the constants used in the definition of D_3 (10). However, we stress again the necessity to use exclusively atoll stations which eliminate the problem of receiver-side acoustic–seismic conversion; in this respect, and because many of its stations were specifically engineered to optimize *T*-phase recording (Talandier & Kuster 1976; Okal 2001), the RSP remains, on a global scale, uniquely suited to this line of research.

The ultimate challenge remains the theoretical justification of the proposed algorithm, which will necessitate systematic modeling of the detailed propagation of hydroacoustic waves generated by a variety of sources, including both explosions in the water column, and dislocations inside the solid Earth, the latter requiring an approach taking into account non-geometrical effects, such as scattering by seafloor heterogeneities.

ACKNOWLEDGEMENTS

REFERENCES

Beutel, E.K. & Okal, E.A., 2003. Strength asperities along oceanic transform faults: a model for the origin of extensional earthquakes on the Eltanin Transform system, *Earth planet. Sci. Lett.*, **216**, 27–41.

Bohnenstiehl, D.R., Scheip, C.R., Matsumoto, H. & Dziak, R.P., 2012. Acoustic variability of air-gun signals recorded at intermediate ranges within the Lau Basin, *Geochem. Geophys. Geosyst.*, **13**(11), Q11013, doi:10.1029/2012GC004337.

de Groot-Hedlin, C.D. & Orcutt, J.A., 1999. Synthesis of earthquake-generated *T* waves, *Geophys. Res. Lett.*, **26**, 1227–1230.

de Groot-Hedlin, C.D. & Orcutt, J.A., 2001. Excitation of *T* phases by seafloor scattering, *J. acoust. Soc. Am.*, **109**, 1944–1954.

Dziak, R.P., 2001. Empirical relationship of *T*-wave energy and fault parameters of northeast Pacific Ocean earthquakes, *Geophys. Res. Lett.*, **28**, 2537–2540.

Ewing, W.M., Jardetzky, W.S. & Press, F., 1957. *Elastic Waves in Layered Media*, McGraw-Hill, 380 pp.

Johnson, R.H., Northrop, J. & Eppley, R., 1963. Sources of Pacific *T* phases, *J. geophys. Res.*, **68**, 4251–4260.

Okal, E.A., 2001. *T*-phase stations for the International Monitoring System of the Comprehensive Nuclear-Test Ban Treaty: a global perspective, *Seismol. Res. Lett.*, **72**, 186–196.

Okal, E.A. & Langenhorst, A.R., 2000. Seismic properties of the Eltanin Transform System, South Pacific, *Phys. Earth planet. Inter.*, **119**, 185–208.

Okal, E.A., Alasset, P.-J., Hyvernaud, O. & Schindelé, F., 2003. The deficient *T* waves of tsunami earthquakes, *Geophys. J. Int.*, **152**, 416–432.

Park, M., Odom, R.I. & Soukup, D.J., 2001. Modal scattering: a key to understanding oceanic *T* waves, *Geophys. Res. Lett.*, **28**, 3401–3404.

Pekeris, C.L., 1948. Theory of propagation of explosive sound in shallow water, *Geol. Soc. Amer. Mem.*, **27**(2), 117 pp.

Piserchia, P.-F., 1998. Propagation et conversion des ondes T par simulation numérique hybride, *Thèse de Doctorat*, Univ. Nice Sophia-Antipolis, 1998.

Reymond, D., Hyvernaud, O., Talandier, J. & Okal, E.A., 2003. *T*-wave detection of two underwater explosions off Hawaii on April 13, 2000, *Bull. seism. Soc. Am.*, **93**, 804–816.

Stephen, R.A. *et al.*, 2013. Deep seafloor arrivals in long-range ocean acoustic propagation, *J. acoust. Soc. Am.*, **134**, 3307–3317.

Taber, J.J. & Lewis, B.T.R., 1986. Crustal structure of the Washington continental margin from refraction data, *Bull. seism. Soc. Am.*, **76**, 1011–1024.

Talandier, J. & Kuster, G.T., 1976. Seismicity and submarine volcanic activity in French Polynesia, *J. geophys. Res.*, **81**, 936–948.

Talandier, J. & Okal, E.A., 1998. On the mechanism of conversion of seismic waves to and from *T* waves in the vicinity of island shores, *Bull. seism. Soc. Am.*, **88**, 621–632.

Talandier, J. & Okal, E.A., 2001. Identification criteria for sources of *T* waves recorded in French Polynesia, *Pure appl. Geophys.*, **158**, 567–603.

Talandier, J., Hyvernaud, O., Okal, E.A. & Piserchia, P.-F., 2002. Long-range detection of hydroacoustic signals from large icebergs in the Ross Sea, Antarctica, *Earth planet. Sci. Lett.*, **203**, 519–534.

Talandier, J., Hyvernaud, O., Reymond, D. & Okal, E.A., 2006. Hydroacoustic signals generated by parked and drifting icebergs in the Southern Indian and Pacific Oceans, *Geophys. J. Int.*, **165**, 817–834.

Tolstoy, I. & Ewing, W.M., 1950. The *T* phase of shallow focus earthquakes, *Bull. seism. Soc. Am.*, **40**, 25–51.

Walker, D.A., McCreery, C.S. & Hiyoshi, Y., 1992. *T*-phase spectra, seismic moments and tsunamigenesis, *Bull. seism. Soc. Am.*, **82**, 1275–1305.

Williams, C.M., Stephen, R.A. & Smith, D.K., 2006. Hydroacoustic events located at the intersection of the Atlantis (30°N) and Kane (23°40′N) Transform Faults with the Mid-Atlantic Ridge, *Geochem. Geophys. Geosyst.*, **7**(6), Q06015, doi:10.1029/2005GC001127.

Yang, Y. & Forsyth, D.W., 2003. Improving epicentral and magnitude estimation of earthquakes from *T* phases by considering the excitation function, *Bull. seism. Soc. Am.*, **93**, 2106–2122.